Journal of Materials Chemistry C

ROYAL SOCIETY OF CHEMISTRY

PAPER

View Article Online
View Journal | View Issue

Cite this: J. Mater. Chem. C, 2026, 14, 2854

Organic thermoelectric films: achieving high conductivity and power factor through sulfonated-poly(3,4-ethylenedioxythiophene) and single-walled carbon nanotube composites

Maël Idir, *[a] Guillaume Chamelot,[a] Yinghui He,[b] Thomas Lemieux,[a] Kendra Bueley,[b] Serge Beaupré,[a] Salima Alem,[b] Jianping Lu,[b] Jean-François Morin[a] and Mario Leclerc †[a]

Received 3rd September 2025,
Accepted 2nd December 2025

DOI: 10.1039/d5tc03290c

rsc.li/materials-c

The quest for sustainable energy solutions is critical amidst environmental challenges. Thermoelectric (TE) devices present a promising approach by converting waste heat into electricity through the Seebeck effect. These devices are advantageous due to their direct energy conversion, solid-state construction, reliability, scalability, long lifespan, and compatibility. However, their efficiency is often low, and they heavily depend on rare, expensive, and toxic inorganic materials. Carbon-based thermoelectric materials, such as carbon allotropes and organic thermoelectric materials such as conductive polymers, offer a sustainable alternative due to their abundance, low cost, eco-friendliness, and high mechanical flexibility, though their efficiency requires improvement. This study explores two generations of thermoelectric materials combining sulfonated-poly(3,4-ethylenedioxythiophene) (PSEDOT), a water-soluble and self-doped polymer, and single-walled carbon nanotubes (SWCNTs). The first generation optimized SWCNT dispersion and purification conditions, while the second generation improved the performance using better materials, resulting in a flexible film with a high conductivity (2000 S cm^{-1}) and a power factor of 96.8 μW m^{-1} K^{-2}.

Introduction

The urgent quest for sustainable energy solutions has become more pressing in the face of environmental challenges. Among the different possibilities, thermoelectric devices offer a promising way to tap into renewable energy from waste heat sources.[1] A thermoelectric generator (TEG) is a heat engine that can produce an electromotive force *via* the Seebeck effect when exposed to a temperature difference. They offer many advantages such as direct energy conversion, solid-state devices with no moving mechanical parts, high reliability, good scalability, interesting lifespan, and high compatibility.[2,3] However, TEG mostly suffers from low efficiency and a high reliance on traditional inorganic materials that are rare, expensive, brittle, rigid, and often contain toxic elements.[4] In this regard, organic thermoelectric materials have emerged as a potential solution due to their abundance, affordability, and potentially renewable nature.[5]

The performance of thermoelectric (TE) materials is evaluated through a dimensionless value called figure of merit (ZT) (eqn (1)). The higher the value, the more efficient the material's conversion capacity. The average reported values are around 1.6 at room temperature with the highest value reaching 2.8 at 1000 K.[6–8] In order to achieve the desired outcome, it is necessary to identify a temperature (T) at which a combination of high Seebeck coefficient (S) and electrical conductivity (σ) values, in conjunction with low thermal conductivity (κ) values, can be attained.

$$ZT = \frac{S^2\sigma}{\kappa}T \quad (1)$$

In order to optimize the figure of merit, it is therefore necessary to adjust all three parameters precisely and simultaneously. However, considering that the thermal conductivity value is generally low for polymers[9] (0.1–0.5 W m^{-1} K^{-1}), the study of these organic thermoelectric materials could be carried out by mainly focusing on the Seebeck effect and electrical conductivity to obtain the power factor (PF) according to the following formula:

$$PF = S^2\sigma \quad (2)$$

[a] Département de Chimie and Centre de recherche sur les matériaux avancés (CERMA), Université Laval, Québec City, Québec G1V 0A6, Canada. E-mail: Mario.Leclerc@chm.ulaval.ca
[b] Quantum and Nanotechnologies Research Centre, National Research Council Canada, Ottawa, Ontario, K1A0R6, Canada
† Director.

This study examines two promising approaches to developing organic thermoelectric materials: conducting polymers and carbon nanotubes (CNTs).[10–15] Both have advantages and disadvantages with respect to thermoelectric applications. On one hand, polymers offer flexibility, low thermal conductivity, and the capacity to adjust their electrical properties, rendering them a versatile candidate for thermoelectric applications. Notable examples could be found among them such as pure polypyrrole (PPy), exhibiting a PF of 0.45 μW m^{-1} K^{-2}, or even doped poly(3-hexylthiophene) (P3HT) with a PF of 27 μW m^{-1} K^{-2}.[16] One of the most commonly used polymers for TE applications is poly(3,4-ethylenedioxythiophene) polystyrene sulfonate (PEDOT : PSS).[17–22] This polymer is also particularly attractive because of its water processability and good electrical conductivity. The highest thermoelectric figure of merit reported for PEDOT : PSS is approximately 0.42 with a power factor of 469 μW m^{-1} K^{-2}. This value was achieved by optimizing the material through post-treatment processes, including the addition of DMSO and ethylene glycol, which enhanced the electrical conductivity and Seebeck coefficient while maintaining low thermal conductivity.[23] Some issues remain regarding the use of PEDOT : PSS, including the use of complex post-treatment processes necessary to limit the influence of the PSS component.

On the other hand, CNTs are highly conductive and stable materials, offering exciting possibilities for energy conversion. Some of the highest *ZT* values achieved for CNT-based materials are in the range of 0.34–0.5.[24] Notably, multi-walled CNT (MWCNT)/Ag_2Se composites have achieved an impressive *ZT* value of around 0.5 at room temperature and a power factor of 533 μW m^{-1} K^{-2}, which are quite high values for carbon-based materials.

However, challenges remain with their synthesis, processing, and cost.[25] The primary challenge in using CNTs for thermoelectric (TE) applications is their poor processability, which often necessitates the use of costly, high-boiling-point solvents. A common solution is to combine CNTs with conjugated polymers, exploiting the polymers' solubility and their strong π–π interactions with the CNTs' sp^2-hybridized carbon scaffold.[26] Significant improvements in the power factor have been observed when combining polymers with CNTs. For example, a single-walled carbon nanotube–polypyrrole (SWCNT-PPy) composite achieved a PF of 37.6 μW m^{-1} K^{-2}, which is three orders of magnitude higher than that of PPy alone. Additionally, a SWCNT-P3HT composite showed a PF of 110 μW m^{-1} K^{-2}, five times greater than that of doped P3HT. These examples demonstrate that the combination of CNTs with polymers can significantly enhance the thermoelectric properties of the polymer while also improving the processability of the CNTs.[16,27]

In this work, two generations of thermoelectric (TE) materials have been developed, involving a mixture of a water-soluble self-doped polymer (PSEDOT), which is a derivative of PEDOT : PSS, and SWCNTs.[28,29] The first generation focused on getting the optimized dispersion conditions and data of the purification process. It also helped find the best conditions for the preparation of free-standing films from this blend. The second generation aimed at enhancing the performance by using starting materials with higher electrical conductivity. This effort led to a flexible and more processable free-standing film with a conductivity of 2000 S cm^{-1} and a power factor of 96.8 μW m^{-1} K^{-2} with good long-term air stability.

Experimental section

Materials

SWCNT samples RN120 (with 10–15% metallic impurities) and XFS16 (99% pure) were purchased from Raymor and used without further purification. Sulfonated-poly(3,4-ethylenedioxythiophene) **P1** (M_w = 20 000 g mol^{-1})[28] and **P2** (M_w = 160 000 g mol^{-1})[29] polymers have been synthesized *via* direct (hetero)arylation polymerization (DHAP) according to the literature (see Fig. 1) with their molecular weight measured by asymmetrical flow field-flow fractionation equipped with a multiangle light scattering detector.[30]

Dispersions of the materials and fabrication of the composite free-standing films

100 mg of polymer was solubilized in 150 mL of deionized water and sonicated for 5–10 min until a homogeneous solution was obtained. 100 mg of SWCNTs was added to the mixture and sonicated for 30 min with a Q-Sonica Ultrasonicator equipped with a 6.4 mm microtip and set at max amplitude (100%). The crude dispersion is then centrifuged for 30 min at 13 000 rpm to separate the dispersed and undispersed SWCNTs. The supernatant was then carefully collected and filtered over a 0.45 μm nylon filter to remove the excess polymer. A free-standing film of the SWCNT/polymer is then peeled off from the filter, washed with chloroform and dried under vacuum at 100 °C for at least 2 h to remove the remaining water.

Characterization

After centrifugation, 10 mL of the supernatant was collected and diluted by a factor of 10. Analyses were then performed on thin films made by dropcasting 100 μL of the diluted composite solution on a silicon wafer. Analyses were also performed on free-standing films. AFM analyses were carried out on an MFP-3D Origin Asylum Research AFM from Oxford Instrument. The analysis was performed in tapping mode and with an AC 160 TS silicon tip. SEM analyses were carried out on a Tescan Vega 3 equipped with a thermionic electron beam (W wire) and with an EDAX Element X-ray probe. Raman spectroscopy analysis was performed on a Bruker (Senterra II) equipped with a 532 nm laser. X-Ray fluorescence (XRF) was carried out on a Rigaku 25X Primus II. Conductivity measurements were conducted on an Ossila four-probe sensing apparatus. For the polymer, thick films were fabricated by drop casting a 1 wt% solution of **P1** or **P2** on a 15 × 15 mm glass substrate. For the composite, measurements were performed directly on the freestanding film when the film was sufficiently robust to withstand the experimental conditions. Three conductivity measurements were obtained for each film, and the resulting values were averaged. The exact polymer mass fraction in G1

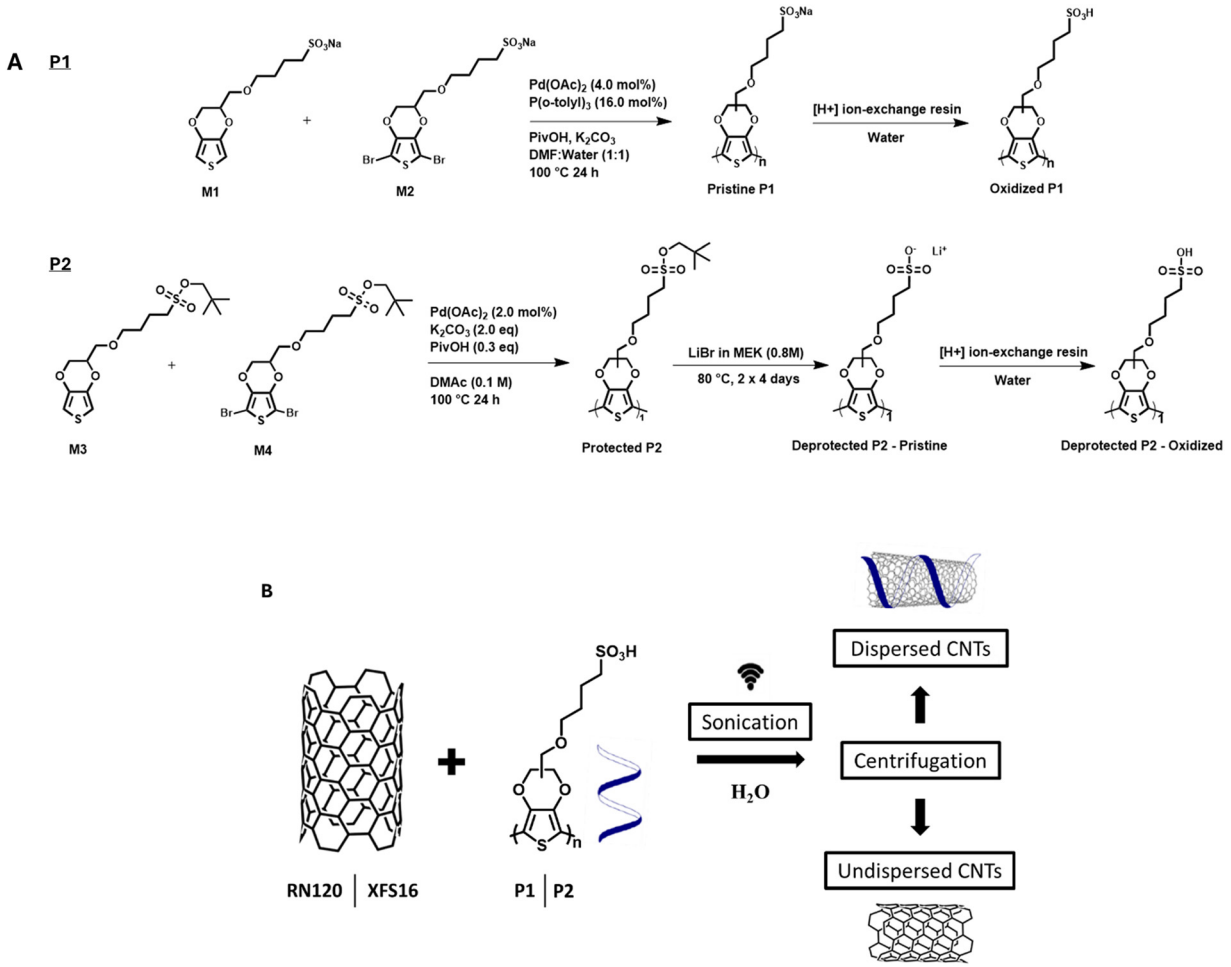

Fig. 1 (A) Synthesis of polymers **P1** and **P2** and (B) protocol of CNT-Polymer dispersion in water.

and G2 could not be determined due to experimental limitations following centrifugation and filtration.

Seebeck measurements and power factor calculations were carried out using a homemade apparatus consisting of two copper blocks separated by a distance of 10 mm. The freestanding composite film was mounted horizontally between copper plates. One side of the copper block was heated using a Peltier device (TE Tech Inc., Model CP-031) with a temperature controller (TE Tech Inc., Model TC-48-20), and the other side was kept at room temperature. The difference in temperature between the two copper blocks ranged from 0 to 50 °C, measured by thermocouples (type K), which were attached to the copper plates and very close to the sample. All the measurements were performed in an ambient atmosphere. Voltage and resistance measurements were recorded using a Keithley Model 2000 multimeter, and digital thermometers (National Instrument, Model USB-TC-01) were used to measure the temperature difference between the two copper blocks. The LabVIEW program was used for controlling the measurement parameters, monitoring, and collecting data.

Additional state-of-the-art techniques such as UV-Vis analysis, fluorescence and thermal conductivity measurements were performed but did not yield any conclusive results (SI).

Results and discussion

Two types of composites have been studied in this work. As shown in Fig. 1, Generation 1 (G1) consisted of the mixing of RN120-SWCNTs with **P1**. RN120-SWCNT contains a 2 : 1 ratio of semiconductor and metallic CNTs and also contains 10–15% of metal impurities coming from a catalytic mixture (iron, nickel, and cobalt) that can, if not removed, influence the electrical properties of the final composite. This raw sample is insoluble in water, making it not processable. However, it is very affordable in terms of production and price due to the absence of tedious purification steps. **P1** was chosen for this study, thanks to two interesting properties. First, the conjugated system of the repeating unit will allow for the formation of π-interactions with the sp^2-hybridized carbon scaffold of CNTs. Also, the presence of sulfonated side chains attached to the repeating unit in **P1** makes the polymer soluble in aqueous medium, while keeping its electrical properties stable for a long period of time. A series of CNT-to-polymer ratios were evaluated in a small-scale experiment. An excess of CNTs did not allow adequate dispersion of the final mixture, which exhibited two distinct phases. Furthermore, an excess of polymer did not yield any discernible improvement compared to a

1 : 1 ratio. The excess polymer was filtered out during purification. Only the 1 : 1 ratio was retained, as observed in the experiments and in good agreement with the literature.[31] This led to the determination of three objectives regarding this generation. First, the combination of the raw nanotubes and the polymer should give a water-dispersed/processable composite. Then, the protocol should show a decrease in the amount of catalytic impurities present in the final product. Finally, the composite should show higher performance regarding the electrical conductivity and thermoelectric properties compared to the polymer alone.

Generation 2 (G2) was designed as a potential upgrade of Generation 1. XFS16 SWCNTs were chosen as an ultra-purified CNT sample (as opposed to the raw RN120 sample) containing a negligible amount of catalytic impurities and composed of only semiconducting CNTs allowing for higher Seebeck coefficient and lower thermal conductivity than metallic CNTs.[32] This implies a significant increase in pricing, but can allow for the fabrication of high-performance materials.[33] **P2** shares the same final structure as **P1**, which makes it also soluble in aqueous medium, but it differs in its synthesis approach, which allows for higher molecular weight and higher conductivities.[29] This also led to the determination of two objectives regarding this generation. Firstly, it ensured that the protocol used could be robust enough to be applied to other CNT samples, and secondly, it ensured that G2 dispersions have better mechanical and electrical properties compared to G1 dispersions. Dispersions D3 (XFS16 + P1) and D4 (RN120 + P2) have also been prepared as controls.

Optical characterization

Raman spectroscopy analyses of the PSEDOT-type polymer and both dispersions G1 and G2 have been performed (Fig. 2). Two broad peaks are observed on the Raman spectrum of the polymer at 1400 cm^{-1} and 2800 cm^{-1}. Those two peaks are then observed on both composite analyses. The presence of a radial breathing mode (RBM) sharp peak at around 250 cm^{-1} in dispersion G1 (Fig. 2A) coupled with a high intensity G band at 1575 cm^{-1}, confirms the presence of both types of CNTs (metallic and semiconducting, respectively) in the final composite.[34]

On the other hand, dispersion G2 (Fig. 2B) only shows an intense G band, confirming the presence of semiconducting CNTs (as described by the manufacturer). The intensity ratio between the D band and the G band (I_D/I_G) gives information about the amount of defects in the CNT structure after the dispersion protocol.[35] In both cases, the I_D/I_G ratios were low (= 0.06), indicating that the final composite does not possess any major defects. This means that the sonication protocol did not affect the electron mobility, so the electrical properties were not degraded.

Atomic force microscopy (AFM) and scanning electron microscopy (SEM) analyses have been performed on both G1 and G2 composite free-standing films (see Fig. 3).

As observed in the AFM results (Fig. 3A) and SEM results (Fig. 3B), the G1 composite exhibits well-defined domains comprising ordered structures (approximately 10 μm in length

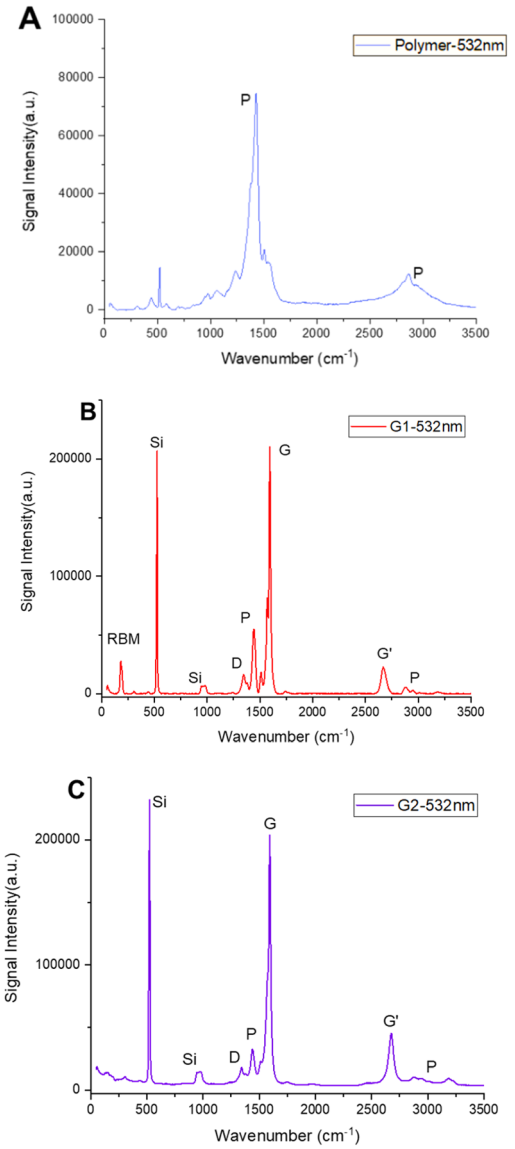

Fig. 2 Raman spectra of the drop-casted films of polymer P1 (A), dispersion G1 (B) and G2 (C) at 532 nm.

with diameters of 3–4 μm), resulting probably from a crystallization phenomenon (a phenomenon appearing only for this combination of polymer and CNT). Crystallization was only qualitative suppositions based on surface morphology observations. XRD analysis regarding this phenomenon couldn't be performed. This resulted in a brittle film not suited for potential flexible applications. In contrast, the G2 composite displays (Fig. 3C and D) an amorphous structure, lacking the presence of well-defined domains. This resulted in a flexible film. As observed in the AFM images, isolated CNTs can be measured at 1–2 μm in length and 10–20 nm in diameter.

Following AFM and SEM analyses, each composite was characterized with a specific technique. XRF was performed on G1 to assess its composition while G2 was analyzed through EDX elemental mapping to assess its atom distribution.

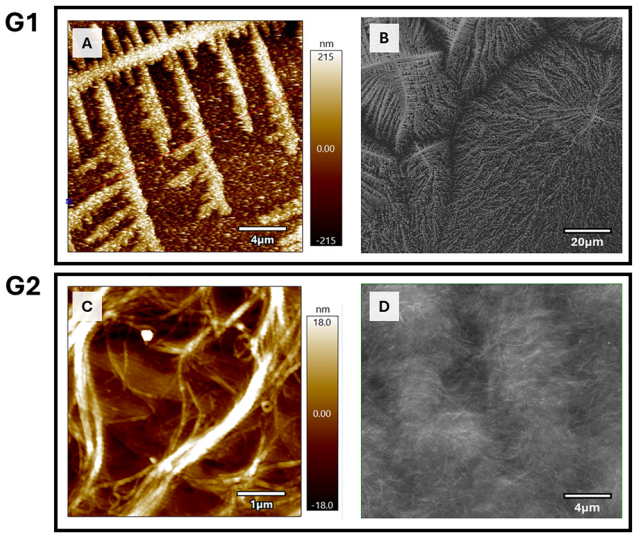

Fig. 3 AFM and SEM analyses of dispersion G1 (A) and (B) and dispersion G2 (C) and (D).

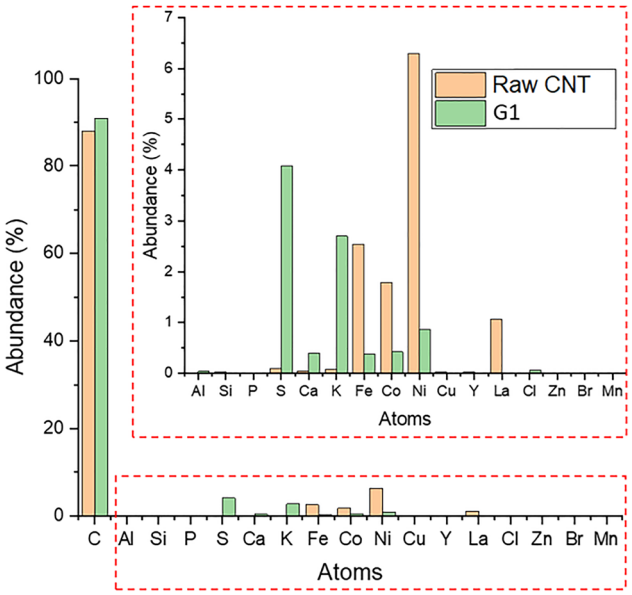

Fig. 4 X-Ray fluorescence of composite G1 and raw RN-120 SWNT.

Fig. 4 presents the results from XRF analysis of the raw sample of SWCNT RN120 (green) and the composite G1 (orange). As mentioned earlier, the RN120-SWCNT sample is not a pure sample. The manufacturer announces the presence of 10–15% of remaining metal catalysts such as iron, nickel and cobalt, which can be seen in the XRF results. After the dispersion and centrifugation, a free-standing film of G1 was analyzed in the same conditions and shows a significative decrease in metal content in the composite going from 10% to 1.7% (Table 1), which implies that the simple protocol used in this study is effective at purifying the RN120-SWNT sample.

Following the analysis of the dispersion of the G2 film in SEM, elemental analysis has been performed to assess the

Table 1 Amount of catalyst impurities in the raw CNT sample RN120 compared to composite G1

Atoms	RN120 (%)	G1 (%)
Fe	2.54	0.38
Co	1.80	0.43
Ni	6.29	0.87
Cu	0.03	0.01
Total	10.66	1.69

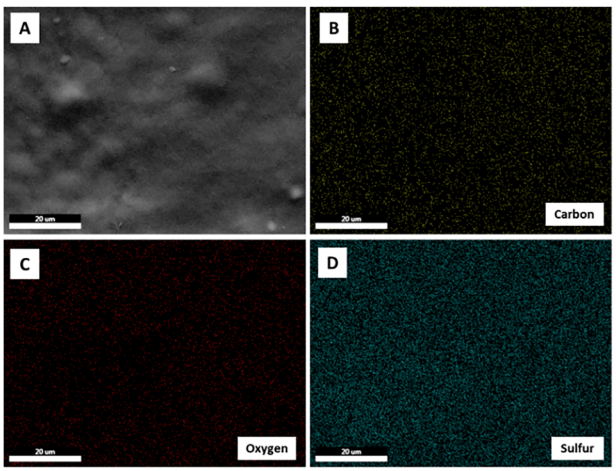

Fig. 5 Elemental mapping of composite G2 exhibiting a uniform distribution of the atom in the freestanding film with (A) the SEM image, (B) the carbon atoms distribution, (C) the oxygen atoms distribution and (D) the sulfur atoms distribution.

distribution of CNTs on the polymer matrix (Fig. 5A). A uniform distribution of carbon (Fig. 5B), oxygen (Fig. 5C) and sulfur (Fig. 5D) atoms has been observed throughout the film without any evidence of clusters. While carbon can be found in both the CNTs and polymer, oxygen and sulfur atoms are only present on the backbone and sidechain of the polymer. These results confirmed the excellent dispersion of CNTs in the polymer matrix giving an amorphous morphology in the composite.

Electrical characterization

An investigation into the electrical properties of free-standing films of composite G1 and G2 has been conducted and is reported in Table 2. Although it exhibits a well-improved electrical conductivity (300 S cm^{-1} for the composite as opposed to 3 S cm^{-1} for the polymer alone) and the highest Seebeck coefficient of all the samples prepared in this work (26 μV K^{-1}), composite G1 displays a smaller power factor compared to other similar systems reported in the literature (green solvent and flexible freestanding film).[31–33] Additionally, the film lacks flexibility, making it unsuitable for flexible thermoelectric applications. In contrast, G2 exhibits the highest electrical conductivity and a power factor that is ten times greater than that of G1, while also demonstrating much better flexibility. It also does not require any post-treatment compared to other types of composites reported in the literature and it only uses a single type of polymer as a dispersing agent.[31,32]

Table 2 Conductivity, Seebeck coefficient and power factor of dispersion G1, G2, D3 and D4

Sample	Solvent	Conductivity (S cm^{-1})	Seebeck coefficient (μV K^{-1})	Power factor (μW m^{-1} K^{-2})	Flexible	Thickness (μm)	Ref.
G1	Water	300	26	9.7	No	80	This work
G2	Water	2000	22	96.8	Yes	80	This work
SWCNT/PEDOT-PSS	Ethanol	900	31	83.9	Yes	—	31
SWCNT/PEDOT-PSS + ionic liquid	Ethanol	1600	33	182.7	—	—	32
Multiwalled + PEDOT : PSS	Ethanol	740	68	339.6	Yes	20	33
Complementary dispersions							
D3	Water	50	nd*	nd*	No	120	This work
D4	Water	670	22	33.2	Yes	80	This work

nd*: not determined.

In order to investigate the origin of the flexibility and the good electrical properties of composite G2, the complementary composite free-standing films of D3 (XFS16 + P1) and D4 (RN120 + P2) have also been prepared. The free-standing film of composite D3 exhibited the lowest electrical conductivity among the samples under investigation. Additionally, the film was the most brittle, which made the Seebeck measurement impossible. In contrast, the free-standing film of D4 demonstrates both flexibility and favorable electrical properties, indicating that the freestanding film characteristics are predominantly influenced by the quality of the polymer used. The improved thermoelectric properties from G1 to G2 can then be attributed to the higher molecular weight of polymer P2, which promotes better charge transport and network homogeneity, resulting in higher electrical conductivity and power factor.

Flexibility and durability testing

Another G2-type dispersion was prepared and subsequently freeze-dried. The resulting powder was then redispersed in water at the appropriate concentration. Next, the solution was blade-coated on a flexible PET substrate (Fig. 6A) to ascertain its durability following a series of bending cycles (Fig. 6B). Subsequently, the electrical conductivity, Seebeck coefficient, and power factor were measured following the blade coating, after 500 bending cycles, and finally seven days after the bending step (Table 3).

This was done to assess the overall stability of the material after deformation. Following the 500 bending cycles, there was a decrease of the electrical conductivity, from 420 to 225 S cm^{-1}, which was attributed to delamination from the film on the PET substrate (Fig. 6C). Despite this decline in performance, the results remained positive and stable over time after the bending step, but there is a clear need for further improvement. A plasma treated or a coated PET substrate and/or the addition of additive in the dispersion could fix the wettability issue and provide a better blade-coated film.

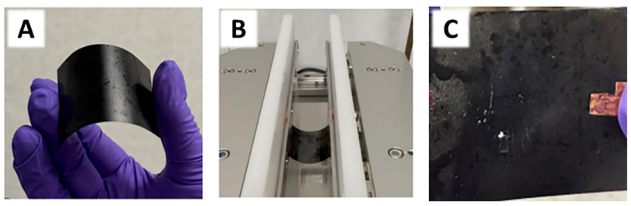

Fig. 6 Flexible testing before and after 500 bending cycles of composite G2 blade-coated onto a PET substrate with (A) the coated film before bending, (B) the film during the bending experiment and (C) the film after bending.

Table 3 Conductivity, Seebeck coefficient and power factor of a G2-type composite blade-coated onto a PET substrate in a flexibility test before and after 500 bending cycles

Film	Thickness (μm)	σ (S cm^{-1})	Seebeck (μV K^{-1})	Power factor (μW m^{-1} K^{-2})
Day 1	3.4	420	23	21.8
Day 1 after 500 bending cycles	3.4	225	20	9
Day 7	3.4	225	20	9

Conclusions

The capacity of the PSEDOT polymer to achieve a stable dispersion of SWCNTs in an aqueous medium has been reported, resulting in the preparation of several freestanding films. The G1 composite, even with its brittle nature and lack of electrical properties compared to the literature, provided crucial information such as the dispersion conditions needed to produce free-standing films in a repeatable manner. The G2 composite demonstrated the highest conductivity, reaching up to 2000 S cm^{-1}, and a power factor of 96.8 μW m^{-1} K^{-2}, which aligns with values reported in the existing literature. Notably, this performance was achieved without any post-treatment, suggesting the potential for further enhancements. The material is also fully water-processable and flexible, making it an excellent candidate for wearable thermoelectric (TE) applications.

Author contributions

All authors have given approval to the final version of the manuscript.

Conflicts of interest

There are no conflicts to declare

Data availability

The data that support the findings of this study are available from the corresponding author, Prof. Jean-François Morin, upon reasonable request.

The data supporting this article have been included as part of the supplementary information (SI). Supplementary information is available. See DOI: https://doi.org/10.1039/d5tc03290c.

Acknowledgements

This work was financially supported by the Natural Sciences and Engineering Research Council of Canada (NSERC) and the Aging in Place Challenge Program at the National Research Council of Canada (NRC).

Notes and references

1 F. Tohidi, S. Ghazanfari Holagh and A. Chitsaz, Thermoelectric Generators: A Comprehensive Review of Characteristics and Applications, *Appl. Therm. Eng.*, 2022, **201**, 117793, DOI: 10.1016/j.applthermaleng.2021.117793.

2 D. Champier, Thermoelectric Generators: A Review of Applications, *Energy Convers. Manage.*, 2017, **140**, 167–181, DOI: 10.1016/j.enconman.2017.02.070.

3 M. A. Zoui, S. Bentouba, J. G. Stocholm and M. Bourouis, A Review on Thermoelectric Generators: Progress and Applications, *Energies*, 2020, **13**(14), 3606, DOI: 10.3390/en13143606.

4 S. LeBlanc, S. K. Yee, M. L. Scullin, C. Dames and K. E. Goodson, Material and Manufacturing Cost Considerations for Thermoelectrics, *Renewable Sustainable Energy Rev.*, 2014, **32**, 313–327, DOI: 10.1016/j.rser.2013.12.030.

5 S. Lee, S. Kim, A. Pathak, A. Tripathi, T. Qiao, Y. Lee, H. Lee and H. Y. Woo, Recent Progress in Organic Thermoelectric Materials and Devices, *Macromol. Res.*, 2020, **28**(6), 531–552, DOI: 10.1007/s13233-020-8116-y.

6 T. C. Harman, P. J. Taylor, M. P. Walsh and B. E. LaForge, Quantum Dot Superlattice Thermoelectric Materials and Devices, *Science*, 2002, **297**(5590), 2229–2232, DOI: 10.1126/science.1072886.

7 M. Rull-Bravo, A. Moure, J. F. Fernández and M. Martín-González, Skutterudites as Thermoelectric Materials: Revisited, *RSC Adv.*, 2015, **5**(52), 41653–41667, DOI: 10.1039/C5RA03942H.

8 Z. Zhou, Y. Huang, B. Wei, Y. Yang, D. Yu, Y. Zheng, D. He, W. Zhang, M. Zou, J.-L. Lan, J. He, C.-W. Nan and Y.-H. Lin, Compositing Effects for High Thermoelectric Performance of Cu2Se-Based Materials, *Nat. Commun.*, 2023, **14**(1), 2410, DOI: 10.1038/s41467-023-38054-y.

9 Y. Jia, Z. Mao, W. Huang and J. Zhang, Effect of Temperature and Crystallinity on the Thermal Conductivity of Semi-Crystalline Polymers: A Case Study of Polyethylene, *Mater. Chem. Phys.*, 2022, **287**, 126325, DOI: 10.1016/j.matchemphys.2022.126325.

10 J. Li, A. B. Huckleby and M. Zhang, Polymer-Based Thermoelectric Materials: A Review of Power Factor Improving Strategies, *J. Materiomics*, 2022, **8**(1), 204–220, DOI: 10.1016/j.jmat.2021.03.013.

11 M. Goel and M. Thelakkat, Polymer Thermoelectrics: Opportunities and Challenges, *Macromolecules*, 2020, **53**(10), 3632–3642, DOI: 10.1021/acs.macromol.9b02453.

12 N. Dubey and M. Leclerc, Conducting Polymers: Efficient Thermoelectric Materials, *J. Polym. Sci., Part B:Polym. Phys.*, 2011, **49**(7), 467–475, DOI: 10.1002/polb.22206.

13 M. Culebras, C. Gómez and A. Cantarero, Review on Polymers for Thermoelectric Applications, *Materials*, 2014, **7**(9), 6701–6732, DOI: 10.3390/ma7096701.

14 S. Iijima, Helical Microtubules of Graphitic Carbon, *Nature*, 1991, 56–58.

15 N. T. Hung, A. R. T. Nugraha and R. Saito, Thermoelectric Properties of Carbon Nanotubes, *Energies*, 2019, **12**(23), 4561, DOI: 10.3390/en12234561.

16 Z. Liu, J. Sun, H. Song, Y. Pan, Y. Song, Y. Zhu, Y. Yao, F. Huang and C. Zuo, High Performance Polypyrrole/SWCNTs Composite Film as a Promising Organic Thermoelectric Material, *RSC Adv.*, 2021, **11**(29), 17704–17709, DOI: 10.1039/D1RA02733F.

17 E. Lim, K. A. Peterson, G. M. Su and M. L. Chabinyc, Thermoelectric Properties of Poly(3-Hexylthiophene) (P3HT) Doped with 2,3,5,6-Tetrafluoro-7,7,8,8-Tetracyanoquinodimethane (F_4 TCNQ) by Vapor-Phase Infiltration, *Chem. Mater.*, 2018, **30**(3), 998–1010, DOI: 10.1021/acs.chemmater.7b04849.

18 Z. Fan and J. Ouyang, Thermoelectric Properties of PEDOT:PSS, *Adv. Elect. Mater.*, 2019, **5**(11), 1800769, DOI: 10.1002/aelm.201800769.

19 Z. Fan, Y. Zhang, L. Pan, J. Ouyang and Q. Zhang, Recent Developments in Flexible Thermoelectrics: From Materials to Devices, *Renewable Sustainable Energy Rev.*, 2021, **137**, 110448, DOI: 10.1016/j.rser.2020.110448.

20 S. Liu, H. Li and C. He, Simultaneous Enhancement of Electrical Conductivity and Seebeck Coefficient in Organic Thermoelectric SWNT/PEDOT:PSS Nanocomposites, *Carbon*, 2019, **149**, 25–32, DOI: 10.1016/j.carbon.2019.04.007.

21 I. Petsagkourakis, S. Riera-Galindo, T.-P. Ruoko, X. Strakosas, E. Pavlopoulou, X. Liu, S. Braun, R. Kroon, N. Kim, S. Lienemann, V. Gueskine, G. Hadziioannou, M. Berggren, M. Fahlman, S. Fabiano, K. Tybrandt and X. Crispin, Improved Performance of Organic Thermoelectric Generators Through Interfacial Energetics, *Adv. Sci.*, 2023, **10**(20), 2206954, DOI: 10.1002/advs.202206954.

22 E. Yvenou, M. Sandroni, A. Carella, M. N. Gueye, J. Faure-Vincent, S. Pouget, R. Demadrille and J.-P. Simonato, Spray-Coated PEDOT:OTf Films: Thermoelectric Properties and Integration into a Printed Thermoelectric Generator, *Mater. Chem. Front.*, 2020, **4**(7), 2054–2063, DOI: 10.1039/D0QM00265H.

23 Q. Wei, M. Mukaida, K. Kirihara, Y. Naitoh and T. Ishida, Recent Progress on PEDOT-Based Thermoelectric Materials, *Materials*, 2015, **8**(2), 732–750, DOI: 10.3390/ma8020732.

24 N. Chen, C. Ren, L. Sun, H. Xue, H. Yang, X. An, X. Yang, J. Zhang and P. Che, Improved Thermoelectric Properties of Multi-Walled Carbon Nanotubes/Ag_2Se *via* Controlling the Composite Ratio, *CrystEngComm*, 2022, **24**(2), 260–268, DOI: 10.1039/D1CE01442K.

25 F. Daneshvar, H. Chen, K. Noh and H.-J. Sue, Critical Challenges and Advances in the Carbon Nanotube–Metal Interface for next-Generation Electronics, *Nanoscale Adv.*, 2021, **3**(4), 942–962, DOI: 10.1039/D0NA00822B.

26 A. G. El-Shamy, Review on the Recent Advance in PEDOT:PSS/Carbonic Fillers Based Nanocomposite for Flexible Thermoelectric Devices and Sensors, *Mater. Today Physics*, 2023, **35**, 101101, DOI: 10.1016/j.mtphys.2023.101101.

27 C. K. Mytafides, L. Tzounis, G. Karalis, P. Formanek and A. S. Paipetis, High-Power All-Carbon Fully Printed and Wearable SWCNT-Based Organic Thermoelectric Generator, *ACS Appl. Mater. Interfaces*, 2021, **13**(9), 11151–11165, DOI: 10.1021/acsami.1c00414.

28 C. Beaumont, J. Turgeon, M. Idir, D. Neusser, R. Lapointe, S. Caron, W. Dupont, D. D'Astous, S. Shamsuddin, S. Hamza, É. Landry, S. Ludwigs and M. Leclerc, Water-Processable Self-Doped Conducting Polymers via Direct (Hetero)Arylation Polymerization, *Macromolecules*, 2021, **54**(12), 5464–5472, DOI: 10.1021/acs.macromol.1c00847.

29 C. Beaumont, T. Lemieux, S. Aivali, M. Hamidzad Sangachin, A. Gasonoo, T. Marcoux St-Pierre, M. Bélanger, S. Beaupré, G. C. Welch and M. Leclerc, Highly Transmissive, Processable, Highly Conducting and Stable Polythiophene Derivatives via Direct (Hetero)Arylation Polymerization, *ACS Macro Lett.*, 2024, 1133–1138, DOI: 10.1021/acsmacrolett.4c00397.

30 M. Idir; J. Gigault and M. Leclerc, Determination Of Conjugated Water-Soluble Polymers Molecular Weight by Asymmetrical Flow Field-Flow Fractionation, unpublished results.

31 H. Song, Y. Qiu, Y. Wang, K. Cai, D. Li, Y. Deng and J. He, Polymer/Carbon Nanotube Composite Materials for Flexible Thermoelectric Power Generator, *Compos. Sci. Technol.*, 2017, **153**, 71–83, DOI: 10.1016/j.compscitech.2017.10.006.

32 Y. Ichinose, A. Yoshida, K. Horiuchi, K. Fukuhara, N. Komatsu, W. Gao, Y. Yomogida, M. Matsubara, T. Yamamoto, J. Kono and K. Yanagi, Solving the Thermoelectric Trade-Off Problem with Metallic Carbon Nanotubes, *Nano Lett.*, 2019, **19**(10), 7370–7376, DOI: 10.1021/acs.nanolett.9b03022.

33 Y. Wang, K. Li, J. Wang, X. Dai, X. Sun, D. Chong, J. Yan, L. Zhang and H. Wang, Green Biopolymer-CNT Films Exhibit High Thermoelectric Power Factor and Electrical Conductivity for Low Temperature Heat Energy Harvesting, *J. Mater. Chem. A*, 2022, **10**(48), 25740–25751, DOI: 10.1039/D2TA07670E.

34 V. Popov, Carbon Nanotubes: Properties and Application, *Mater. Sci. Eng., R*, 2004, **43**(3), 61–102, DOI: 10.1016/j.mser.2003.10.001.

35 *Micromechanics and Nanomechanics of Composite Solids*, ed. S. A. Meguid and G. J. Weng, Springer International Publishing, Cham, 2018, DOI: 10.1007/978-3-319-52794-9.